



**HAL**  
open science

## Layer-by-Layer modification of graphite felt with MWCNT for vanadium redox flow battery

Mathieu Etienne, Jose F Vivo-Vilches, Ivan Vakulko, Claire Genois, Liang Liu, Michel Perdicakis, Rolf Hempelmann, Alain Walcarius

### ► To cite this version:

Mathieu Etienne, Jose F Vivo-Vilches, Ivan Vakulko, Claire Genois, Liang Liu, et al.. Layer-by-Layer modification of graphite felt with MWCNT for vanadium redox flow battery. *Electrochimica Acta*, 2019, 313, pp.131-140. 10.1016/j.electacta.2019.04.022 . hal-02149600

**HAL Id: hal-02149600**

**<https://hal.univ-lorraine.fr/hal-02149600v1>**

Submitted on 27 Nov 2020

**HAL** is a multi-disciplinary open access archive for the deposit and dissemination of scientific research documents, whether they are published or not. The documents may come from teaching and research institutions in France or abroad, or from public or private research centers.

L'archive ouverte pluridisciplinaire **HAL**, est destinée au dépôt et à la diffusion de documents scientifiques de niveau recherche, publiés ou non, émanant des établissements d'enseignement et de recherche français ou étrangers, des laboratoires publics ou privés.

# Layer-by-Layer modification of graphite felt with MWCNT for vanadium redox flow battery

Mathieu Etienne,<sup>1,\*</sup> Jose F. Vivo-Vilches,<sup>1</sup> Ivan Vakulko,<sup>1</sup> Claire Genois,<sup>1</sup> Liang Liu,<sup>1</sup> Michel Perdicakis,<sup>1</sup> Rolf Hempelmann,<sup>2,3</sup> Alain Walcarius<sup>1</sup>

<sup>1</sup> Université de Lorraine, CNRS, LCPME, F-54000 Nancy, France.

<sup>2</sup> Physical Chemistry, Campus B2.2, Saarland University, D-66123 Saarbrücken, Germany

<sup>3</sup> KIST Europe, Saarbrücken, Germany

\*Corresponding author: [mathieu.etienne@univ-lorraine.fr](mailto:mathieu.etienne@univ-lorraine.fr) (M. Etienne)

Tel : +33 (0) 3 72 74 73 82 Fax : +33 (0) 3 83 27 54 44

## **Abstract**

Layer-by-Layer (LbL) deposition of multi-walled carbon nanotubes (MWCNT) was used to modify porous electrodes for vanadium redox flow batteries. Preliminary studies performed over glassy carbon electrodes (GCEs) showed that assemblies obtained with MWCNT displayed better mechanical stability than those prepared with other carbon nanoforms. The LbL process involved successive deposition of a positively-charged polymer (in our case polyethylenimine, PEI) and carbon nanotubes modified in such a way to get their surface negatively-charged, and it was found that the use of MWCNT dispersed with poly(acrylic acid) (PAA) allowed a faster and more homogenous film growth than –COOH functionalized SWCNT. The thickness of the MWCNT assembly deposited onto a GCE strongly influenced the electrochemistry of  $\text{VO}^{2+}/\text{VO}_2^+$  species. The thicker the film, the better the electrochemical reversibility resulted. An electron transfer rate constant  $k_0$  of  $5 \times 10^{-4} \text{ cm s}^{-1}$  was determined for the electrode prepared with one hundred bi-layers and treated at  $650 \text{ }^\circ\text{C}$  in inert atmosphere. After optimizing the process on GCEs, the LbL technique was applied to the modification of graphite felt electrodes (GFEs). GF electrodes modified with ten bilayers of PEI-PAA(MWCNT) were tested in a vanadium redox flow battery, showing a net decrease in the charge and discharge overpotentials with respect to the unmodified graphite felt. Lower overpotentials for charge-discharge resulted in higher energy and voltage efficiencies for the battery with modified GF electrodes. Furthermore, cyclability of the system was tested and no fading was observed in the battery performance after one hundred cycles.

**Keywords:** vanadium redox flow battery, layer-by-layer deposition, carbon electrodes, carbon nanotubes, graphite felt.

## 1. Introduction

The demand for renewable energy, e.g. electricity produced from sun or wind, is actually increasing significantly with the goal to become less dependent from fossil reserves or nuclear plants. The major drawback of renewable energies is their discontinuous production, varying dramatically with time, which makes the estimation of production unreliable. Moreover, the periods of production do not necessarily fit the periods of consumption [1]. Therefore, the development of renewable energy must be associated to the development of suitable battery technologies displaying low cost, long life-cycle and low maintenance [1,2]. Redox-flow batteries are promising devices to exhibit such features [3,4].

Redox-flow batteries (RFB) have the characteristic to dissociate the reservoirs for storage of anolyte and catholyte from the electrochemical cell, allowing rapid charging and discharging of the redox species [5–8]. Main components of the battery are the ion-permeable membrane and the electrodes, these latter being the focus of the present study. Different redox species can be involved in RFB. All-vanadium batteries, the most-successful commercial approach to date, involve only vanadium species in both catholyte and anolyte [3,4]. It allows minimizing the risk of irreversible mixing of electrolyte in case of defects/cracks or undesired permeability in the membrane separator. Two redox couples are involved in all-vanadium batteries, respectively  $V(\text{III})/V(\text{II})$  and  $V(\text{V})/V(\text{IV})$  [8–12]. Studies dealing with the optimization of the electrode material for improving battery performance usually focus on increasing the electron transfer rate of the redox reactions, especially those involved in the anode compartment  $V(\text{V})/V(\text{IV})$  which is the kinetic limitation. Such improvement can be reached by increasing the electrode surface area and/or by chemical surface modification [13–16]. In this respect, carbon materials have been widely used for RFB optimization [13–18]. Carbon clothes or graphite felt, after activation, display interesting properties for electrochemical conversion of vanadium species [19–22]. Additional modifications can be

implemented, like metal [21,23,24], metal oxide deposition [25–27] or incorporation of heteroatoms such as oxygen, nitrogen or phosphorous [14–16,28–33].

It is already known that carbon nanomaterials, i.e. graphite [19–21], carbon nanotube [34–39], graphene [28,40,41] or graphene oxide [42–44], are likely to improve the electrochemical reversibility of vanadium species redox reactions. The developed electroactive surface area and the presence of functionalities such as hydroxyl and carboxyl groups [32,44] or the sp<sup>2</sup> carbon content on the surface are important parameters that can improve the performance of the battery [45]. Nevertheless, carbon or graphite felt electrodes displaying a large porous volume that facilitates mass transport of the electrolytes into the electrochemical cell are still a key component in redox flow batteries [14,29,37,46].

Previous reports in the literature described first attempts to get the combination of the graphite felt with carbon nanotubes [30,34–36,38,39,47] or reduced graphene [42,44]. The method usually involved impregnation of the graphite felt with carbon nanostructures and further drying of the material. One issue here is to reach homogeneous deposition of the carbon nanomaterial over the whole surface of the graphite felt fibers while maintaining its internal porosity in order to benefit from the electrocatalytic properties of these materials without losing the mass transport properties of the felt.

Layer-by-layer (LbL) assembly is a process that utilizes different attractions between deposited species to create thin films of controlled thickness and properties [48,49]. These films are most often created by alternately exposing positively and negatively charged constituents (solid particles or organic polymers), from dilute aqueous suspensions or solutions, to a charged or polar substrate. Each pair of deposited species (consisting of two individual constituents) is referred to as a bi-layer (BL) and can range in thickness from few nm to more than 100 nm thick depending on chemistry, molecular weight of the component, temperature, counter-ion, ionic strength, and pH [50–53].

This process can be used to create functional thin films offering a wide range of applications including optical-to-electric power conversion, magnetic sensing and lithium battery electrolytes [54–56]. The LbL process has many advantages over other coating methods, including ease of processing, precise control of thickness and composition of the assembly, and applicability to deposition of rather uniform coatings on surfaces of complex morphologies. For example, LbL was already used by Grunlan and co-workers to prepare conductive carbon-based composite films [57,58] and [carbon nanotubes – polyelectrolyte]-based sensors [59].

In the present study, we have evaluated the interest of the LbL assembly method to modify carbon-based electrodes with carbon nanomaterials (nanoparticles, nanotubes) that could be used in vanadium redox flow batteries. From preliminary experiments on flat carbon plates, it rapidly came out that the best results were obtained with multi-walled carbon nanotubes (MWCNT) and polymers. This most promising approach was thus exploited to grow layers of MWCNT on the inner surface of a highly porous graphite felt electrode in a controlled manner. Optimization was made step-by-step, on the basis of systematic deposition on flat glassy carbon surface, and after that on the graphite felt electrodes (composed of graphitized carbon fibers). The purpose of this work is to demonstrate the influence of the assembly parameters and the carbon layer characteristics on the electrochemistry of  $\text{VO}^{2+}/\text{VO}_2^+$  and the related battery performance. Special focus was given to provide a simple method likely to be scalable on large electrode surfaces for possible implementation in operational redox flow batteries.

## **2. Experimental section**

### *2.1. Reagents*

Multi-walled carbon nanotubes (MWCNT, length: 5  $\mu\text{m}$ , diameter: 6-9 nm) were purchased from Sigma-Aldrich. Single-walled carbon nanotubes functionalized with carboxyl

groups (SWCNT-COOH) were obtained from Nanolab (MA, USA). Carbon black powder (Ketjenblack-EC 600 JD) was kindly provided by Akzo Chemie, Netherlands. Poly(ethylene imine) (PEI) 50 % (w/v) water solution, poly(acrylic acid) (PAA) 35 % wt. solution in water, sulfuric acid 98 % and vanadium(III) chloride 97 % ( $\text{VCl}_3$ ) were purchased from Sigma-Aldrich and vanadium(IV) oxide sulfate hydrate 99.9 % ( $\text{VO}_2\text{SO}_4 \cdot x\text{H}_2\text{O}$ ) by Alfa Aesar. Glassy carbon plates (SIGRADUR G-plates  $1 \times 12 \times 20$  mm) were obtained from HTW Hochtemperatur-Werkstoffe GmbH and graphite felt (GFD 4.6 E.A.) from SGL Group (properties, Table S1). All solutions were prepared with high purity water ( $18 \text{ M}\Omega \text{ cm}$ ) from a Purelab Option water purification system (Elga).

## *2.2. Preparation of solutions and suspensions for LbL deposition*

The PEI solution ( $1 \text{ mg mL}^{-1}$ ) was prepared by dilution of a commercial aqueous solution of PEI (50 % (w/v)), which was then used to form the positively charged layers. Negatively charged layers were prepared from suspensions of either MWCNT or carbon black powder (CB) in PAA, or using a suspension of SWCNT-COOH. To prepare the PAA-based suspensions, the commercial polymeric solution (35 % wt. in water) was diluted to obtain 100 mL of solution containing  $1 \text{ mg mL}^{-1}$  PAA, to which 100 mg of MWCNT or CB were added and dispersed by ultrasonication for 15 min. The suspension of functionalized nanotubes was prepared by dispersion of 100 mg of SWCNT-COOH in 100 mL of water under ultrasonication for 15 min. In case of multiple uses, all suspensions have been sonicated again for 15 min prior to use.

## *2.3. Electrode pre-treatment and Layer-by-Layer deposition*

The LbL process involves the adsorption of a first layer of a positively charged material (PEI) onto the electrode surface, a washing step, and the deposition of a negatively charged

overlayer (PAA) driven by the favorable electrostatic interactions with the underlying positively charged component, and further washing with water. This allows the sequential growth of multiple bi-layers by alternating the deposition of PEI and PAA.

To optimize the LbL deposition several approaches were tested in the GCE. First attempts were made to disperse various amounts of carbon nanotubes (MWCNT) in a PEI solution [43,60], but it was rapidly observed that the resulting PEI(MWCNT) suspensions were not stable. PEI was thus used alone to deposit the positively charged layers and to enable a better control of the film growth process.

For the deposition of the carbon nanomaterials-based negatively charged layer, different systems were investigated: a suspension containing only SWCNT functionalized with carboxyl groups (SWCNT-COOH); carbon black particles dispersed in poly(acrylic acid) (PAA(CB)); and finally, multi-walled carbon nanotubes dispersed in PAA solution, leading to negatively charged particles (PAA(MWCNT)) as described in the literature [43,60]. Glassy carbon electrodes (GCE) were cleaned and polished using 600 and 1200 grit papers, and then using aqueous slurries of alumina powders (50 nm) on a polishing micro-cloth. These experiments were performed by means of an automatic 3 axis moving system made in the laboratory. The system was programmed to introduce the GCE, alternately in the three suspensions/solutions (PEI suspension, carbon nanomaterial suspension, and water - washing solution). The protocol was repeated up to reach a defined number of bi-layers on the electrode surface and samples were kept in each cup for 1 min. From these experiments with GCE, it was concluded that the most promising system resulted the one based on the assembly of bi-layers made of PEI and PAA(MWCNT), and therefore this protocol was employed to obtain functionalized GF electrodes.

In the case of graphite felts (GF), these electrodes were activated by thermal treatment at 400 °C for 30 hours under air atmosphere before impregnation in order to improve their

wettability and conductivity, according to the procedure found in literature [19]. The principle of modification was basically the same as for the GCE, however longer contact times between the material and the suspensions/solution were necessary and an additional convection was applied, either by forcing the suspensions/solutions to flow through the felt or by mechanical stirring. The contact time between the GF electrodes and the suspensions was 20 min and it was repeated 10 times. After deposition and washing with water, the samples were slowly dried under air atmosphere by heating from room temperature to 80 °C for 5 hours in an oven. The deposits were then thermally treated at 650 °C under nitrogen atmosphere, for 1 h (GCE) or 2 h (graphite felt electrodes).

#### *2.4. Physicochemical Characterization and Battery test*

Samples morphology was characterized by scanning electron microscopy (SEM, Hitachi FEG S4800). Measurements of the thickness for the layers deposited on glassy carbon were conducted using the profilometry function of a home-built scanning electrochemical microscope (SECM) operating with a shear force control of the tip-to-sample distance [61]). X-ray photoelectron spectroscopy (XPS) analysis on graphite felt samples was performed with a KRATOS AXIS Ultra DLD.

Cyclic voltammetry experiments were performed with a SP 150 Biologic potentiostat (Grenoble, France) in a three-electrode cell containing a 0.15 M VOSO<sub>4</sub> solution in H<sub>2</sub>SO<sub>4</sub> 3 M as electrolyte, the modified/unmodified carbon material (glassy carbon or graphite felt) as working electrode, an Ag/AgCl as reference electrode and a carbon rod as counter-electrode. The quantitative analysis of cyclic voltammetric curves recorded at various scan rates (from 10 to 200 mV s<sup>-1</sup>) allows to estimate the electron transfer rate constant,  $k_0$ , on the basis of Randles-Sevcik (Equation S1) and Butler-Volmer equations (Equations S2 and S3) [62,63].

Battery tests and Electrochemical Impedance Spectroscopy (EIS) were performed using a home-designed redox flow battery (Figure S1) with cavities for electrodes of 0.4 cm × 2 cm × 7 cm (14 cm<sup>2</sup> of apparent surface area). Both activated graphite felt and MWCNT functionalized graphite felt were tested as electrodes. For EIS measurements, the system was immersed in 3 M H<sub>2</sub>SO<sub>4</sub>, and the cell was closed. The measurements were carried out at open circuit potential (OCP) in a frequency range from 0.1 Hz to 100 kHz with a sinusoidal potential amplitude of 10 mV.

In the case of charge-discharge experiments the system was fed with the electrolyte from two recipients containing 20 mL a 50/50 stoichiometric mixture of V(III) and V(IV) at 1.5 M prepared by diluting the appropriated amounts of VCl<sub>3</sub> and VOSO<sub>4</sub> in 3 M H<sub>2</sub>SO<sub>4</sub> which was recirculated at a flow rate of 20 mL min<sup>-1</sup>. Nafion® 115 (purchased from Ion Power, Germany) was used as the ion-exchange membrane. Polarization curves were obtained up to 1.2 V at a scan rate of 5 mV s<sup>-1</sup> before charge-discharge experiments. Then several charge-discharge cycles at several current densities (20, 50 and 80 mA cm<sup>-2</sup>) were performed, followed by one hundred charge-discharge cycles at 20 mA cm<sup>-2</sup> in order to test the cyclability of the system.

### **3. Results and discussion**

#### *3.1. Physico-chemical characterization.*

SEM micrographs were recorded respectively before and after modification, to confirm the successful deposition of PEI-PAA(MWCNT) bi-layers in the felt electrode. Figure 1 depicts a view of one fiber of the felt (A) before modification and (B) after coverage with 10 PEI-PAA(MWCNT) bi-layers and pyrolysis. These images show successful deposition of MWCNT in the form of a quite uniform layer onto the carbon fiber (Figure 1B). The quantity of deposited materials was however found larger at the periphery of the felt (Figure 1C) than on the fibers situated in the center of the electrode (Figure 1D). Even if the thickness of the MWCNT layer

is difficult to estimate, the defects/cracks induced during SEM sample preparation enable ones to conclude that deposits onto the felt surface are thinner ( $< 1 \mu\text{m}$ ) than on GCE ( $1.7 \mu\text{m}$  for 10 bi-layers, Figure S3). Deposition of MWCNT was thus less effective on graphite felt than on the glassy carbon, because of the restricted motion of the slurries used for LbL deposition into the porous carbon electrode.

XPS analyses were performed on the pristine graphite felt (curve a, Figure 2A), air activated graphite felt at  $400 \text{ }^\circ\text{C}$  for 30 hours (curve b, Figure 2A), and functionalized graphite felt after deposition of 10 bi-layers of PEI-PAA(MWCNT) and pyrolysis (curve c, Figure 2A). The corresponding surface chemical compositions are presented in Table 1 (deconvolution of  $\text{C}_{1s}$  signal is provided in Figure S4 of the Supplementary Material). In agreement with the literature [19], the oxygen content at the surface of the graphite felt was increased (from 3.0 to 5.7 %) after thermal activation, due to the formation of oxidized groups on the carbon surface. The deposition of 10 bi-layers of MWCNT, and their subsequent pyrolysis at  $650 \text{ }^\circ\text{C}$ , results also in slightly higher oxygen content (6.0 %) and the presence of an additional nitrogen contribution (2.0 %) is also evidenced, originated from PEIs moieties. A magnification of the  $\text{N}_{1s}$  signal on the sample modified with MWCNT is shown in Figure 2B. These two signals can be attributed to pyridinic N (398.2 eV) and pyrrolic N (400.1 eV) and no graphitic N (401.3 eV) was detected, in good agreement with results reported elsewhere [29]. The carbon type was also dramatically modified by the deposition of MWCNT as illustrated by the variation of the  $\text{sp}^2$  content (Table 1), from 62.5% for the thermally activated graphite felt to more than 73 % after MWCNT deposition. This is consistent with the fact that the  $\text{sp}^2$ -C content correlates with the conductivity of the carbon, as electrons are transported along the delocalized p-orbitals [45], contributing to explain better performance of the MWCNT modified felt electrodes.

### *3.2. Electrochemistry of vanadium species on GCE electrodes.*

After characterizing the surface chemistry and morphology of materials, their electrocatalytic performance for vanadium electrochemistry was evaluated by means of Cyclic Voltammetry. When comparing results for un-modified and modified GCEs, it can be observed that in the absence of MWCNT, the electrochemical response was characterized by a low electron transfer rate as evidenced by a peak potential difference close to 0.4 V (curve a, Figure 3A). The number of bi-layers has also a strong influence on the electrochemical behavior of the electrode after their pyrolysis (Figure 3). The deposition of 5 and 10 bi-layers (BL) led to a dramatic decrease of  $\Delta E_p$ , i.e., down to 178 mV for 10 BL (curve b, Figure 3A). A further increase on the number of BL led then to a continuous, yet slower, decrease of  $\Delta E_p$  values (Figure 3B), down to 110 mV for 100 BL (curve c, Figure 3A). Thus, it was decided that 10 BL were proper for the GFE functionalization, since a further deposition could lead to restrictions in the mobility of the electrolyte along the porosity of the material.

It is also important to remark the needing of the thermal treatment, since a poor electrochemical response was observed in the presence of 0.15 M  $VO^{2+}$  in 3 M  $H_2SO_4$  after L-b-L deposition (curve a, Figure 4A). The presence of polyelectrolytes will reduce the conductivity of glassy carbon surface so it is necessary to treat it thermally in order to graphitize and stabilize the film. Treatments have been performed under nitrogen atmosphere at various temperatures ranging from 450 to 850 °C for 1 hour. As illustrated for the film treated at 650 °C (see curve b in Figure 4A), well defined redox peaks can be obtained for the  $VO^{2+}/VO_2^+$  redox system. Actually, one can qualitatively analyze the efficiency of the thermal treatment on the electron transfer kinetics via a measurement of the anodic-to-cathodic peak potentials separation ( $\Delta E_p$ ). As shown on Figure 4B, the lowest  $\Delta E_p$  value was obtained for 650 °C, which is thus the optimal temperature ensuring the effective graphitization of the organic polymers, ensuring thereby an efficient electron transfer between vanadyl species and the electrode. Higher temperature led to the degradation of the MWCNT assembly, while a lower temperature

was not sufficient to convert the polymer from the film into carbon. For instance, a treatment at 850 °C in these conditions led to the complete degradation of the MWCNT layer and no electrochemical reaction could be observed (see curve c in Figure 4A).

The critical influence of MWCNT on the electrochemical response to vanadium species has been largely discussed in the literature [29,34,35,37], however we only found one work resulting in quantitative analysis of this electrochemical reaction [64]. The quantitative analysis of cyclic voltammetric curves recorded at various scan rates allows to estimate the electron transfer rate constant,  $k_0$ , on the basis of Randles-Sevcik and Butler-Volmer equations [62,63]. A value of  $k_0 = 5 \times 10^{-4} \text{ cm s}^{-1}$  was obtained for the sample prepared with 100 BL, from CV curves recorded at various scan rates and corresponding plots of peak currents,  $i_p$ , versus square root of scan rate and  $\ln(i_p)$  versus potential (see details in Supplementary Material, Figures S5-7 and associated discussion). This value is in the same range of magnitude as or higher than kinetic data reported for electrochemistry of vanadium species with different carbon materials [13,65–67]. All these results point out the interest of applying LbL assembly for the fabrication of active electrode surface likely to be used in vanadium redox flow battery application.

### 3.3. Electrochemistry of vanadium species on GFE electrodes.

After demonstrating the improvement on the  $\text{VO}^{2+}/\text{VO}_2^+$  electrochemistry by the LbL functionalization, as well as, optimizing the pyrolysis temperature and the number of BL for GCEs modification with PEI-PAA(MWCNT), the cyclic voltammograms were obtained for GF based electrodes. When results for air activated graphite felt are compared with the one for functionalized graphite felt, a considerable improvement on electrode performance can be observed (Figure 5). The graphite felt electrode activated at 400 °C for 30 hours under air atmosphere showed a peak separation  $\Delta E=0.38\text{V}$  between oxidation and reduction signals (curve a), while for the one modified with 10 bi-layers of MWCNT, this potential separation

decreased down to 0.26 V. Moreover, the cathodic current recorded on reversal scan increased significantly from -51 mA to -86 mA (curve b). All these features indicate that the modification of the graphite felt with MWCNT contributes to enhance the electron transfer rates of the  $\text{VO}^{2+}/\text{VO}_2^+$  redox couple, and therefore, a better performance of these materials as electrodes for the battery is expected. Consistently with observation made on GCE (Figure 4B), a thermal at 750 °C led to a degradation of the electrochemical performances, as it is illustrated in curve c of Figure 5 that shows that the peak separation was increased up to  $\Delta E=0.68$  V.

### 3.4. Vanadium redox flow battery.

The functionalized material was finally tested in a battery setup designed in our laboratory (see Figure S1 in the Supplementary Material). We first performed impedance characterization of the battery (Figure 6A) in the presence of activated graphite felt (curve a) and in the presence of graphite felt modified by MWCNT in 3 M  $\text{H}_2\text{SO}_4$ . The fitting results are provided in Supplementary Materials (Figure S8, Table S2). At high frequency, the DC resistance of these two systems was not significantly different, indicating that the incorporation of MWCNT did not significantly alter the electronic conductivity of the graphite felt. As compared with the unmodified graphite felt, the MWCNT loaded felt showed much lower  $R_{ct}$  values, suggesting that the electroactive surface area of the felt was enhanced. Besides, a capacitive element was observed in the MWCNT-loaded felt, suggesting that the LbL modification might make the graphite felt suitable as capacitive material.

The influence of the MWCNT on the electrochemical response was found critical in terms of improving the battery performance. Figure 6B shows the polarization curves in the presence of 1.5 M V(III)/V(IV) electrolyte with batteries filled with (a) the original graphite felt electrode or (b) the MWCNT-modified one. The current started to increase in the presence

of MWCNT at much lower potential than in their absence, the difference being larger than 800 mV at current densities below  $10 \text{ mA cm}^{-2}$ .

Charge-discharge experiments demonstrated the effectiveness of the LbL functionalization of GF. As depicted in the previous section, the potential for the V(IV) oxidation reaction to occur was lower in the case of MWCNT functionalized sample, as well as the difference between the anodic and the cathodic peak potential (Figure 5). This is clearly reflected in the charge-discharge experiments (Figure 7) performed at low current density tested ( $20 \text{ mA cm}^{-2}$ ). With activated graphite felt, the initial charging potential was closed to 1.4 V (curve a of Figure 7A). The process started at much lower potential with MWCNT modified graphite felt, between 0.8 and 0.9 V (curve b of Figure 7A). This difference is ascribed not only to the more efficient oxidation of V(IV) to V(V), but also to the faster reduction of the vanadium species on the modified electrode than on the unmodified electrode. After 1 hours, the potential of both batteries became similar, but after several cycles, the advantage of the modified graphite felt becomes obvious (Figure 7A). Figure 7B reports the efficiencies of the two batteries, with graphite felt (dashed line) or with MWCNT modified graphite felt (continuous). The major difference is observed in the voltage efficiency (blue lines) that is improved by more than five percent in the presence of MWCNT. A small difference in coulombic efficiency (green lines) was also observed in these conditions, leading to an improvement of the energy efficiency (red lines).

Figure 8A reports the long stability of the modified electrode while charging/discharging at 20, 50 and  $80 \text{ mA cm}^{-2}$ . The battery was first tested during 39 cycles, showing an energy efficiency of 83 % at  $20 \text{ mA cm}^{-2}$ , 73 % at  $50 \text{ mA cm}^{-2}$  and 62 at  $80 \text{ mA cm}^{-2}$ . At cycle 39, a polarization curve was performed and the experiment was reinitialized. This polarization curve reported in Figure 6B (curve c) is showing that the current was lower after 39 cycles than at the very beginning of the experiment (curve b of Figure 6B), but still

significantly higher than the current measured with graphite felt in the battery cell (curve a of Figure 6B). This decrease in the current measured in the polarization curve could be due to small degradation of the electrode or by the state of charge of the electrolyte. The charging-discharging cycles were then reinitialized, with using slightly lower limits for the charge and the discharge processes (Figure 7A), leading to stable energy efficiency of 85 % at  $20 \text{ mA cm}^{-2}$  over 100 cycles.

Finally, we compared the efficiency of the battery with activated GF as electrodes over more than 100 cycles, at 20, 50 and  $80 \text{ mA cm}^{-2}$  (Figure S9). The coulombic efficiencies were similar for both electrodes, however, the lower potential needed to start the charging for the functionalized electrode and the shorter difference between charging and discharging onset potentials led to much higher energy voltage efficiencies for this electrode compared to activated GF (Figure S9B). This difference increases as the current density does being nearly 8 % at  $20 \text{ mA cm}^{-2}$ , more than 20 % at  $50 \text{ mA cm}^{-2}$ , and around 30 % at  $80 \text{ mA cm}^{-2}$  (Figure S9B). These results confirmed that the LbL protocol depicted in this paper is an excellent procedure to obtain functionalized GF based electrodes.

#### 4. Conclusions

Layer-by-layer assembly can be applied for modification of carbon electrodes with MWCNT in order to enhance the electron transfer rates of redox species involved in all-vanadium redox flow batteries. The polyelectrolyte used to assemble MWCNT needs to be converted into carbon by pyrolysis under nitrogen atmosphere prior to use. The temperature of treatment strongly influenced the electrochemical behavior of vanadium species and an optimum at  $650 \text{ }^\circ\text{C}$  was found. Increasing the number of bi-layers improved significantly the reversibility of  $\text{VO}^{2+}/\text{VO}_2^+$  redox couple, especially up to 10 BLs. An electron transfer rate constant of  $5 \times 10^{-4} \text{ cm s}^{-1}$  was determined in the best conditions. After optimizing the conditions

on a system where the functionalization process was faster (glassy carbon electrodes), the method was successfully applied to the modification of porous graphite felt electrodes. XPS analysis after MWCNT deposition shows a significant increase in the  $sp^2$  carbon proportion on the surface and the presence of O and N groups from MWCNT, polyethyleneimine and polyacrylic acid.

Modified graphite felt electrodes showed a better electrochemical performance on vanadium electrolyte, needing a lower potential for the oxidation reaction of V(IV) to V(V) and lowering the difference between the cathodic and the anodic peaks as well as increasing their intensities. This was also reflected in the battery tests; modified GF electrodes presented higher energy and voltage efficiencies and this performance was not lost after several charge-discharge cycles. Therefore, this work demonstrates the benefits of layer-by-layer functionalization of graphite felt electrodes with PEI-PAA(MWCNT) for all-vanadium redox flow batteries.

### **Acknowledgements**

This work has been financially supported by the UE-FEDER Interreg IV-A program (RFB-Solar project). We acknowledge Lisa Salsi for SEM imaging (SCMEM, Université de Lorraine), Aurélien Renard for XPS measurements and Jean-Paul Moulin for the help in construction of the different accessories for layer-by-layer deposition and the battery cells.

### **5. Bibliography**

- [1] Z. Yang, J. Zhang, M.C.W. Kintner-Meyer, X. Lu, D. Choi, J.P. Lemmon, J. Liu, Electrochemical energy storage for green grid., *Chem. Rev.* 111 (2011) 3577–613. doi:10.1021/cr100290v.
- [2] B. Dunn, H. Kamath, J.M. Tarascon, Electrical energy storage for the grid: a battery of

- choices., *Science*. 334 (2011) 928–35. doi:10.1126/science.1212741.
- [3] M. Skyllas-Kazacos, J.F. McCann, Vanadium redox flow batteries (VRBs) for medium- and large-scale energy storage, in: Woodhead Publishing, 2015: pp. 329–386. doi:10.1016/B978-1-78242-013-2.00010-8.
- [4] G. Kear, A.A. Shah, F.C. Walsh, Development of the all-vanadium redox flow battery for energy storage: a review of technological, financial and policy aspects, *Int. J. Energy Res.* 36 (2012) 1105–1120. doi:10.1002/er.1863.
- [5] M.R. Palacín, Recent advances in rechargeable battery materials: a chemist's perspective., *Chem. Soc. Rev.* 38 (2009) 2565–2575. doi:10.1039/b820555h.
- [6] C. Ponce de León, A. Frías-Ferrer, J. González-García, D.A. Szánto, F.C. Walsh, Redox flow cells for energy conversion, *J. Power Sources*. 160 (2006) 716–732. doi:10.1016/j.jpowsour.2006.02.095.
- [7] P. Leung, X. Li, C. Ponce de León, L. Berlouis, C.T.J. Low, F.C. Walsh, Progress in redox flow batteries, remaining challenges and their applications in energy storage, *RSC Adv.* 2 (2012) 10125. doi:10.1039/c2ra21342g.
- [8] M. Skyllas-Kazacos, M.H. Chakrabarti, S.A. Hajimolana, F.S. Mjalli, M. Saleem, Progress in Flow Battery Research and Development, *J. Electrochem. Soc.* 158 (2011) R55. doi:10.1149/1.3599565.
- [9] C. Minke, T. Turek, Materials, system designs and modelling approaches in techno-economic assessment of all-vanadium redox flow batteries – A review, *J. Power Sources*. 376 (2018) 66–81. doi:10.1016/J.JPOWSOUR.2017.11.058.
- [10] M. Ulaganathan, V. Aravindan, Q. Yan, S. Madhavi, M. Skyllas-Kazacos, T.M. Lim, Recent Advancements in All-Vanadium Redox Flow Batteries, *Adv. Mater. Interfaces*. 3 (2016) 1500309. doi:10.1002/admi.201500309.
- [11] M. Park, J. Ryu, J. Cho, Nanostructured Electrocatalysts for All-Vanadium Redox

- Flow Batteries, *Chem. - An Asian J.* 10 (2015) 2096–2110.  
doi:10.1002/asia.201500238.
- [12] C. Choi, S. Kim, R. Kim, Y. Choi, S. Kim, H. Jung, J.H. Yang, H.T. Kim, A review of vanadium electrolytes for vanadium redox flow batteries, *Renew. Sustain. Energy Rev.* 69 (2017) 263–274. doi:10.1016/J.RSER.2016.11.188.
- [13] M.H. Chakrabarti, N.P. Brandon, S. a. Hajimolana, F. Tariq, V. Yufit, M. a. Hashim, M. a. Hussain, C.T.J. Low, P.V. Aravind, Application of carbon materials in redox flow batteries, *J. Power Sources.* 253 (2014) 150–166.  
doi:10.1016/j.jpowsour.2013.12.038.
- [14] M. Park, J. Ryu, Y. Kim, J. Cho, Corn protein-derived nitrogen-doped carbon materials with oxygen-rich functional groups : a highly efficient electrocatalyst for all-vanadium redox flow batteries, *Energy Environ. Sci.* 7 (2014) 3727–3735.  
doi:10.1039/C4EE02123A.
- [15] L. Wu, Y. Shen, L. Yu, J. Xi, X. Qiu, Boosting vanadium flow battery performance by Nitrogen-doped carbon nanospheres electrocatalyst, *Nano Energy.* 28 (2016) 19–28.  
doi:10.1016/j.nanoen.2016.08.025.
- [16] J. Kim, H. Lim, J. Jyoung, E. Lee, J.S. Yi, D. Lee, High electrocatalytic performance of N and O atomic co-functionalized carbon electrodes for vanadium redox flow battery, *Carbon* 111 (2017) 592–601. doi:10.1016/j.carbon.2016.10.043.
- [17] A. Di Blasi, O. Di Blasi, N. Briguglio, A.S. Aricò, D. Sebastián, M.J. Lázaro, G. Monforte, V. Antonucci, Investigation of several graphite-based electrodes for vanadium redox flow cell, *J. Power Sources.* 227 (2013) 15–23.  
doi:10.1016/j.jpowsour.2012.10.098.
- [18] M. Rychcik, M. Skyllas-Kazacos, Evaluation of electrode materials for vanadium redox cell, *J. Power Sources.* 19 (1987) 45–54. doi:10.1016/0378-7753(87)80006-X.

- [19] B. Sun, M. Skyllas-Kazacos, Modification of graphite electrode materials for vanadium redox flow battery application—I. Thermal treatment, *Electrochim. Acta.* 37 (1992) 1253–1260. doi:10.1016/0013-4686(92)85064-R.
- [20] B. Sun, M. Skyllas-Kazacos, Chemical modification of graphite electrode materials for vanadium redox flow battery application—part II. Acid treatments, *Electrochim. Acta.* 37 (1992) 2459–2465. doi:10.1016/0013-4686(92)87084-D.
- [21] B. Sun, M. Skyllas-Kazacos, Chemical modification and electrochemical behaviour of graphite fibre in acidic vanadium solution, *Electrochim. Acta.* 36 (1991) 513–517. doi:10.1016/0013-4686(91)85135-T.
- [22] C. Flox, C. Fàbrega, T. Andreu, A. Morata, M. Skoumal, J. Rubio-Garcia, J.R. Morante, Highly electrocatalytic flexible nanofiber for improved vanadium-based redox flow battery cathode electrodes, *RSC Adv.* 3 (2013) 12056. doi:10.1039/c3ra40463c.
- [23] W.H. Wang, X.D. Wang, Investigation of Ir-modified carbon felt as the positive electrode of an all-vanadium redox flow battery, *Electrochim. Acta.* 52 (2007) 6755–6762. doi:10.1016/j.electacta.2007.04.121.
- [24] B. Li, M. Gu, Z. Nie, Y. Shao, Q. Luo, X. Wei, X. Li, J. Xiao, C. Wang, V. Sprenkle, W. Wang, Bismuth Nanoparticle Decorating Graphite Felt as a High-Performance Electrode for an All-Vanadium Redox Flow Battery, *Nano Lett.* 13 (2013) 1330–1335. doi:10.1021/nl400223v.
- [25] C. Busacca, O. Di Blasi, N. Briguglio, M. Ferraro, V. Antonucci, A. Di Blasi, Electrochemical performance investigation of electrospun urchin-like V<sub>2</sub>O<sub>3</sub>-CNF composite nanostructure for vanadium redox flow battery, *Electrochim. Acta.* 230 (2017) 174–180. doi:10.1016/j.electacta.2017.01.193.
- [26] A. Di Blasi, C. Busaccaa, O. Di Blasia, N. Briguglioa, G. Squadritoa, V. Antonuccia,

- Synthesis of flexible electrodes based on electrospun carbon nanofibers with Mn<sub>3</sub>O<sub>4</sub> nanoparticles for vanadium redox flow battery application, *Appl. Energy*. 190 (2017) 165–171. doi:10.1016/j.apenergy.2016.12.129.
- [27] X. Ma, P. Kolla, Y. Zhao, A.L. Smirnova, H. Fong, Electrospun lignin-derived carbon nanofiber mats surface-decorated with MnO<sub>2</sub> nanowhiskers as binder-free supercapacitor electrodes with high performance, *J. Power Sources*. 325 (2016) 541–548. doi:10.1016/j.jpowsour.2016.06.073.
- [28] L. Shi, S. Liu, Z. He, J. Shen, Nitrogen-Doped Graphene: Effects of nitrogen species on the properties of the vanadium redox flow battery, *Electrochim. Acta*. 138 (2014) 93–100. doi:10.1016/j.electacta.2014.06.099.
- [29] S. Wang, X. Zhao, T. Cochell, A. Manthiram, Nitrogen-Doped Carbon Nanotube/Graphite Felts as Advanced Electrode Materials for Vanadium Redox Flow Batteries, *J. Phys. Chem. Lett.* 3 (2012) 2164–2167. doi:10.1021/jz3008744.
- [30] D.S. Yang, J.Y. Lee, S.W. Jo, S.J. Yoon, T.H. Kim, Y.T. Hong, Electrocatalytic activity of nitrogen-doped CNT graphite felt hybrid for all-vanadium redox flow batteries, *Int. J. Hydrogen Energy*. 43 (2018) 1516–1522. doi:10.1016/j.ijhydene.2017.11.145.
- [31] Z. He, Y. Jiang, J. Zhu, Y. Li, L. Dai, W. Meng, L. Wang, S. Liu, Phosphorus Doped Multi-Walled Carbon Nanotubes: An Excellent Electrocatalyst for the VO<sup>2+</sup>/VO<sub>2</sub><sup>+</sup> Redox Reaction, *ChemElectroChem*. (2018). doi:10.1002/celec.201800438.
- [32] C. Noh, S. Moon, Y. Chung, Y. Kwon, Chelating functional group attached to carbon nanotubes prepared for performance enhancement of vanadium redox flow battery, *J. Mater. Chem. A*. 5 (2017) 21334–21342. doi:10.1039/C7TA06672D.
- [33] K.J. Kim, S.W. Lee, T. Yim, J.G. Kim, J.W. Choi, J.H. Kim, M.-S. Park, Y.J. Kim, A new strategy for integrating abundant oxygen functional groups into carbon felt

- electrode for vanadium redox flow batteries, *Sci. Rep.* 4 (2015) 6906.  
doi:10.1038/srep06906.
- [34] W. Li, J. Liu, C. Yan, Modified multiwalled carbon nanotubes as an electrode reaction catalyst for an all vanadium redox flow battery, *J. Solid State Electrochem.* 17 (2013) 1369–1376. doi:10.1007/s10008-013-2006-6.
- [35] W. Li, J. Liu, C. Yan, Multi-walled carbon nanotubes used as an electrode reaction catalyst for  $\text{VO}_2^+/\text{VO}^{2+}$  for a vanadium redox flow battery, *Carbon* 49 (2011) 3463–3470. doi:10.1016/j.carbon.2011.04.045.
- [36] W. Li, J. Liu, C. Yan, The electrochemical catalytic activity of single-walled carbon nanotubes towards  $\text{VO}_2^+/\text{VO}^{2+}$  and  $\text{V}^{3+}/\text{V}^{2+}$  redox pairs for an all vanadium redox flow battery, *Electrochim. Acta.* 79 (2012) 102–108.  
doi:10.1016/j.electacta.2012.06.109.
- [37] G. Wei, C. Jia, J. Liu, C. Yan, Carbon felt supported carbon nanotubes catalysts composite electrode for vanadium redox flow battery application, *J. Power Sources.* 220 (2012) 185–192. doi:10.1016/j.jpowsour.2012.07.081.
- [38] M.Z. Jelyani, S. Rashid-Nadimi, S. Asghari, Treated carbon felt as electrode material in vanadium redox flow batteries: a study of the use of carbon nanotubes as electrocatalyst, *J. Solid State Electrochem.* 21 (2017) 69–79. doi:10.1007/s10008-016-3336-y.
- [39] I. Mustafa, A. Al Shehhi, A. Al Hammadi, R. Susantyoko, G. Palmisano, S. Almheiri, Effects of carbonaceous impurities on the electrochemical activity of multiwalled carbon nanotube electrodes for vanadium redox flow batteries, *Carbon* 131 (2018) 47–59. doi:10.1016/J.CARBON.2018.01.069.
- [40] J. Jin, X. Fu, Q. Liu, Y. Liu, Z. Wei, K. Niu, J. Zhang, Identifying the active site in nitrogen-doped graphene for the  $\text{VO}_2^+/\text{VO}_2^{(+)}$  redox reaction., *ACS Nano.* 7 (2013)

- 4764–73. doi:10.1021/nn3046709.
- [41] C. Flox, J. Rubio-García, R. Nafria, R. Zamani, M. Skoumal, T. Andreu, J. Arbiol, A. Cabot, J.R. Morante, J. Ramon, Active nano-CuPt<sub>3</sub> electrocatalyst supported on graphene for enhancing reactions at the cathode in all-vanadium redox flow batteries, *Carbon* 50 (2012) 2372–2374. doi:10.1016/j.carbon.2012.01.060.
- [42] Z. González, C. Botas, C. Blanco, R. Santamaría, M. Granda, P. Álvarez, R. Menéndez, Thermally reduced graphite and graphene oxides in VRFBs, *Nano Energy*. 2 (2013) 1322–1328. doi:10.1016/j.nanoen.2013.06.014.
- [43] Z. González, C. Botas, C. Blanco, R. Santamaría, M. Granda, P. Álvarez, R. Menéndez, Graphite oxide-based graphene materials as positive electrodes in vanadium redox flow batteries, *J. Power Sources*. 241 (2013) 349–354. doi:10.1016/j.jpowsour.2013.04.115.
- [44] W. Li, J. Liu, C. Yan, Reduced graphene oxide with tunable C/O ratio and its activity towards vanadium redox pairs for an all vanadium redox flow battery, *Carbon* 55 (2013) 313–320. doi:10.1016/j.carbon.2012.12.069.
- [45] J. Melke, P. Jakes, J. Langner, L. Riekehr, U. Kunz, Z. Zhao-Karger, A. Nefedov, H. Sezen, C. Wöll, H. Ehrenberg, C. Roth, Carbon materials for the positive electrode in all-vanadium redox flow batteries, *Carbon* 78 (2014) 220–230. doi:10.1016/j.carbon.2014.06.075.
- [46] X.L. Zhou, T.S. Zhao, L. An, Y.K. Zeng, L. Wei, Critical transport issues for improving the performance of aqueous redox flow batteries, *J. Power Sources*. 339 (2017) 1–12. doi:10.1016/J.JPOWSOUR.2016.11.040.
- [47] Y. Munaiah, S. Suresh, S. Dheenadayalan, V.K. Pillai, P. Ragupathy, Comparative Electrocatalytic Performance of Single-Walled and Multiwalled Carbon Nanotubes for Zinc Bromine Redox Flow Batteries, *J. Phys. Chem. C*. 118 (2014) 14795–14804. doi:10.1021/jp503287r.

- [48] P. Bertrand, A. Jonas, A. Laschewsky, R. Legras, Ultrathin polymer coatings by complexation of polyelectrolytes at interfaces: suitable materials, structure and properties, *Macromol. Rapid Commun.* 21 (2000) 319–348. doi:10.1002/(SICI)1521-3927(20000401)21:7<319::AID-MARC319>3.0.CO;2-7.
- [49] G. Decher, J.B. Schlenoff, *Multilayer Thin Films—Sequential Assembly of Nanocomposite Materials*, Wiley–VCH, Weinheim, Germany, 2003.
- [50] H. Zhang, J. R uhe, Interaction of Strong Polyelectrolytes with Surface-Attached Polyelectrolyte Brushes—Polymer Brushes as Substrates for the Layer-by-Layer Deposition of Polyelectrolytes, *Macromolecules.* 36 (2003) 6593–6598. doi:10.1021/ma020830s.
- [51] O. Mermut, C.J. Barrett, Effects of Charge Density and Counterions on the Assembly of Polyelectrolyte Multilayers, *J. Phys. Chem. B.* 107 (2003) 2525–2530. doi:10.1021/jp027278t.
- [52] R.A. McAloney, M. Sinyor, V. Dudnik, M.C. Goh, Atomic Force Microscopy Studies of Salt Effects on Polyelectrolyte Multilayer Film Morphology, *Langmuir.* 17 (2001) 6655–6663. doi:10.1021/la010136q.
- [53] Z. Sui, D. Salloum, J.B. Schlenoff, Effect of Molecular Weight on the Construction of Polyelectrolyte Multilayers: Stripping versus Sticking, *Langmuir.* 19 (2003) 2491–2495. doi:10.1021/la026531d.
- [54] F. Hua, T. Cui, Y.M. Lvov, Ultrathin Cantilevers Based on Polymer–Ceramic Nanocomposite Assembled through Layer-by-Layer Adsorption, *Nano Lett.* 4 (2004) 823–825. doi:10.1021/nl0498031.
- [55] Z. Liang, K.L. Dzienis, J. Xu, Q. Wang, Covalent Layer-by-Layer Assembly of Conjugated Polymers and CdSe Nanoparticles: Multilayer Structure and Photovoltaic Properties, *Adv. Funct. Mater.* 16 (2006) 542–548. doi:10.1002/adfm.200500334.

- [56] D.M. DeLongchamp, P.T. Hammond, Highly ion conductive poly(ethylene oxide)-based solid polymer electrolytes from hydrogen bonding layer-by-layer assembly., *Langmuir*. 20 (2004) 5403–11.
- [57] C. Jason Jan, M.D. Walton, E.P. McConnell, W.S. Jang, Y.S. Kim, J.C. Grunlan, Carbon black thin films with tunable resistance and optical transparency, *Carbon* 44 (2006) 1974–1981. doi:10.1016/j.carbon.2006.01.021.
- [58] M.D. Walton, Y.S. Kim, C.J. Jan, E.P. McConnel, W.N. Everett, J.C. Grunlan, Deposition and patterning of conductive carbon black thin films, *Synth. Met.* 157 (2007) 632–639. doi:10.1016/j.synthmet.2007.07.002.
- [59] B. Kumar, Y.T. Park, M. Castro, J.C. Grunlan, J.F. Feller, Fine control of carbon nanotubes-polyelectrolyte sensors sensitivity by electrostatic layer by layer assembly (eLbL) for the detection of volatile organic compounds (VOC)., *Talanta*. 88 (2012) 396–402. doi:10.1016/j.talanta.2011.11.006.
- [60] M. Govindan, I. Moon, Improved Electrochemical Preparation of Nano Porous-Graphene Oxide Edge Like Electrode for Cerium / Vanadium Redox Flow Batteries, *Int. J. Electrochem. Sci.* 8 (2013) 12172–12183.
- [61] M. Etienne, B. Layoussifi, T. Giornelli, D. Jacquet, SECM-based automate equipped with a shearforce detection for the characterization of large and complex samples, *Electrochem. Commun.* 15 (2012) 70–73. doi:10.1016/j.elecom.2011.11.028.
- [62] A.J. Bard, L.R. Faulkner, *Electrochemical methods: fundamentals and applications*, 2nd ed., John Wiley & Sons, Inc, 2001.
- [63] E. Sum, M. Skylas-Kazacos, A study of the V(II)/V(III) redox couple for redox flow cell applications, *J. Power Sources*. 15 (1985) 179–190. doi:10.1016/0378-7753(85)80071-9.
- [64] J. Friedl, C.M. Bauer, A. Rinaldi, U. Stimming, Electron transfer kinetics of the –

Reaction on multi-walled carbon nanotubes, *Carbon* 63 (2013) 228–239.

doi:10.1016/j.carbon.2013.06.076.

- [65] X.W. Wu, T. Yamamura, S. Ohta, Q.X. Zhang, F.C. Lv, C.M. Liu, K. Shirasaki, I. Satoh, T. Shikama, D. Lu, S.Q. Liu, Acceleration of the redox kinetics of  $\text{VO}_2^+/\text{VO}_2$  and  $\text{V}^{3+}/\text{V}^{2+}$  couples on carbon paper, *J. Appl. Electrochem.* 41 (2011) 1183–1190.  
doi:10.1007/s10800-011-0343-7.
- [66] T. Yamamura, N. Watanabe, T. Yano, Y. Shiokawa, Electron-Transfer Kinetics of  $\text{Np}^{3+}/\text{Np}^{4+}$ ,  $\text{NpO}_2^+/\text{NpO}_2^{2+}$ ,  $\text{V}^{2+}/\text{V}^{3+}$ , and  $\text{VO}_2^+/\text{VO}_2$  at Carbon Electrodes, *J. Electrochem. Soc.* 152 (2005) A830–A836.
- [67] W. Wang, X. Fan, J. Liu, C. Yan, C. Zeng, Temperature-related reaction kinetics of the vanadium(IV)/V redox couple in acidic solutions, *RSC Adv.* 4 (2014) 32405.  
doi:10.1039/C4RA04278F.

## Figure captions

**Figure 1.** Scanning electron micrograph of one fiber of a graphite felt observed (A) before and (B) after modification with 10 PEI-PAA(MWCNT) bi-layers. (C) Periphery and (D) center of the graphite felt electrode after modification with 10 PEI-PAA(MWCNT) bi-layers. The sample has been treated at 650 °C under nitrogen atmosphere.

**Figure 2.** (A) XPS spectra of (a) the pristine graphite felt, (b) the activated graphite felt and (c) the graphite felt modified with 10 PEI-PAA(MWCNT) bi-layers and treated at 650 °C under inert atmosphere. (B) Narrow N<sub>1s</sub> XPS spectrum of the graphite felt modified with 10 PEI-PAA(MWCNT) bi-layers and treated at 650 °C under inert atmosphere. The binding energy from pyridinic N at 398.2 eV and pyrrolic N at 400.1 eV are indicated on the graph.

**Figure 3.** (A) Cyclic voltammograms recorded at 5 mV·s<sup>-1</sup> in presence of solution containing 0.15 M VOSO<sub>4</sub> and 3 M H<sub>2</sub>SO<sub>4</sub>, using (a) an unmodified GCE and GCE modified with (b) 10 and (c) 100 bi-layers of PEI-PAA(MWCNT). (B) Variation of the anodic-to-cathodic peak potential differences as a function of the number of PEI-PAA(MWCNT) bi-layers on the electrodes. All electrodes were treated at 650 °C under nitrogen atmosphere prior to use.

**Figure 4.** (A) Cyclic voltammograms recorded in the same conditions as in Fig. 3 using GCE modified with 10 PEI-PAA(MWCNT) bi-layers, respectively (a) before thermal treatment and after treatment at (b) 650 °C or (c) 850 °C. (B) Variation of the anodic-to-cathodic peak potential differences as a function of treatment temperature.

**Figure 5.** (A) Cyclic voltammograms recorded in the same conditions as in Fig. 3, using (a) an activated graphite felt electrode, and (b&c) a graphite felt modified with 10 bi-layers of PEI-PAA(MWCNT) and treated at (b) 650 °C and (c) 750 °C.

**Figure 6.** (A) Electrochemical Impedance Spectroscopy characterization in 3 M H<sub>2</sub>SO<sub>4</sub> of the battery cell prepared with (a) graphite felt and (b) graphite felt modified with MWCNT. (B)

Polarization curves using (a) an activated graphite felt electrode and (b and c) a graphite felt modified with MWCNT. Curve b has been measured before the first run of the battery test and curve c before the second run of the battery.

**Figure 7.** (A) Charge-discharge experiments at  $20 \text{ mA cm}^{-2}$  with (a) graphite felt and (b) graphite felt modified with MWCNT. (B) Coulombic (green), energy (red) and voltage (blue) efficiency along several charge-discharge cycles for (dashed) graphite felt and (continuous) graphite felt modified with MWCNT.

**Figure 8.** (A) Charge-discharge experiments at 20, 50 and  $80 \text{ mA cm}^{-2}$  using MWCNT functionalized graphite felt. A first experiment has been performed (blue curve) before the experiment was continued with different charge-discharge potential limits (black curve).

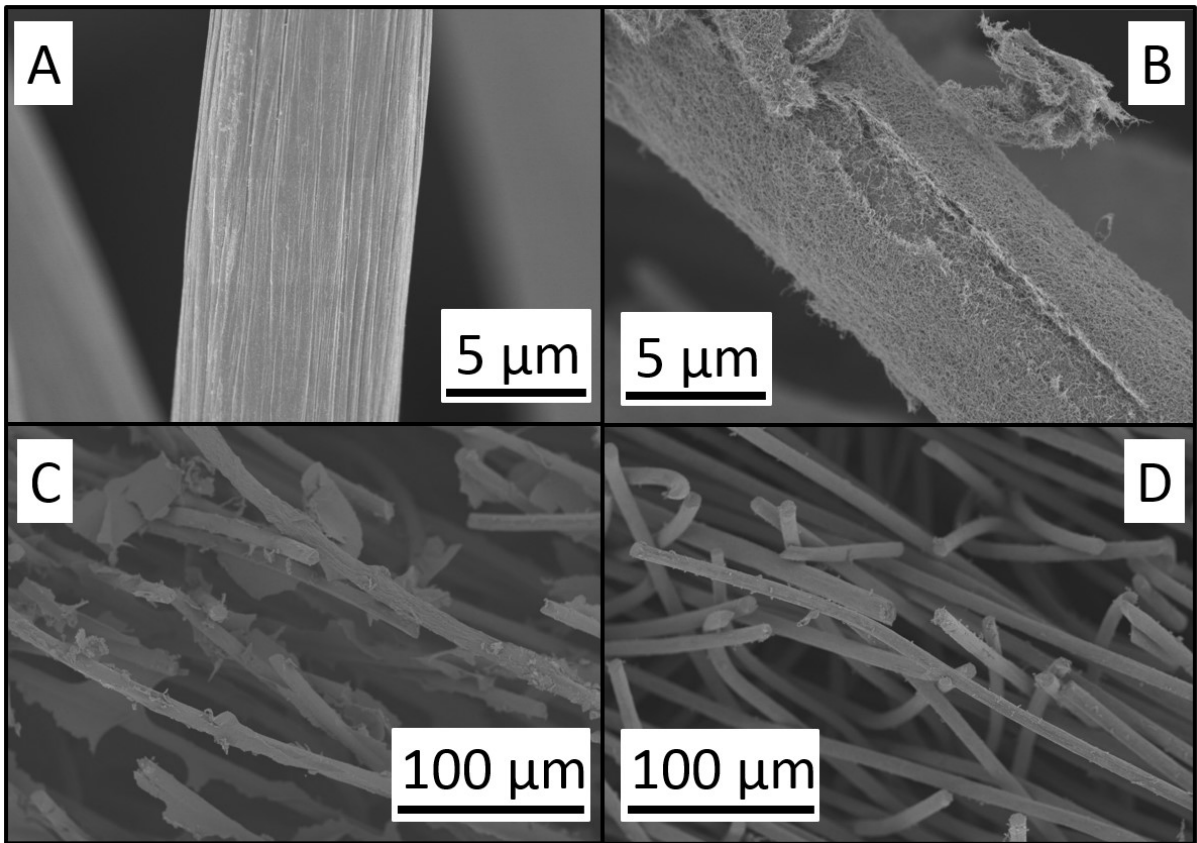


Figure 1

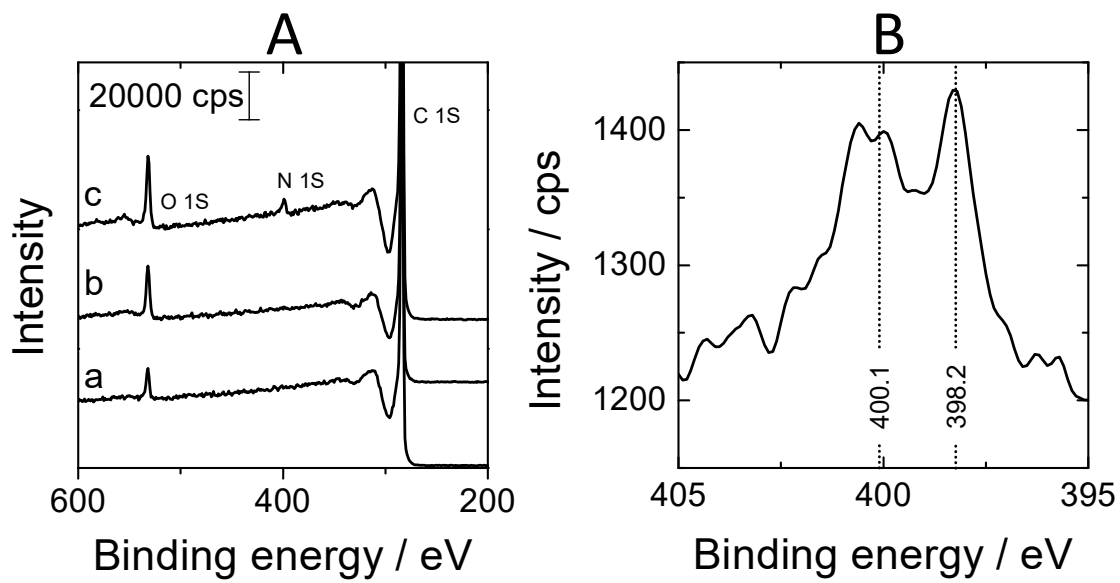


Figure 2

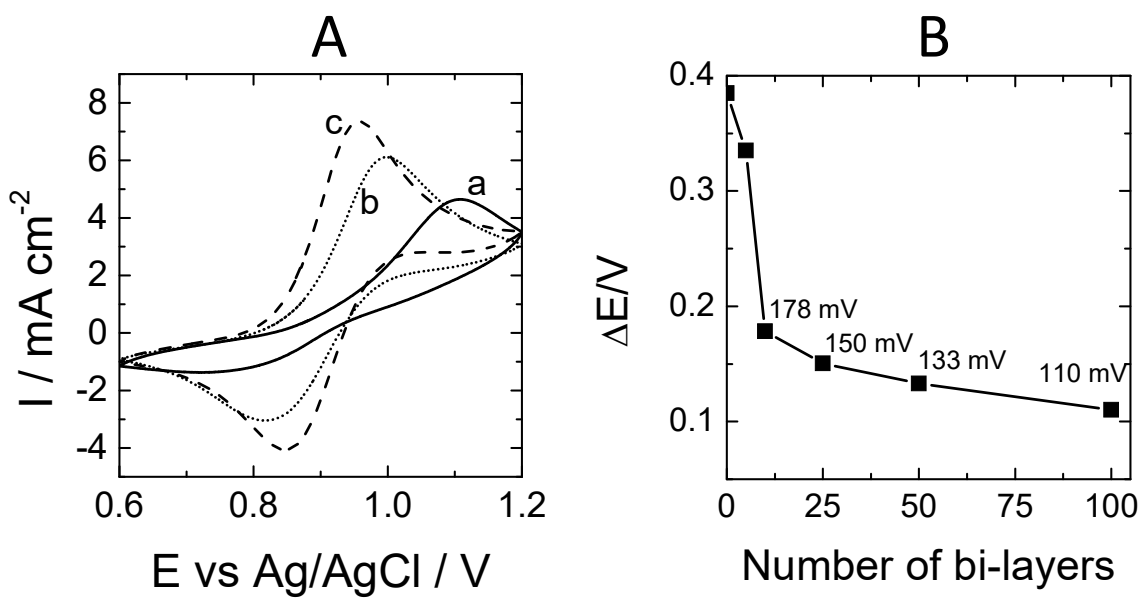


Figure 3

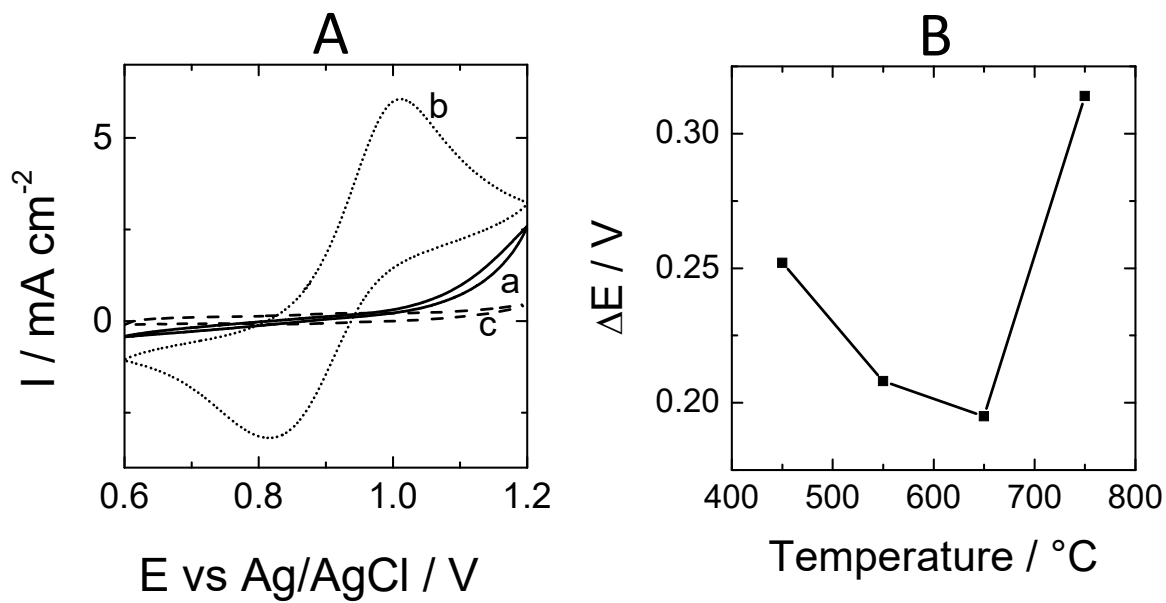


Figure 4

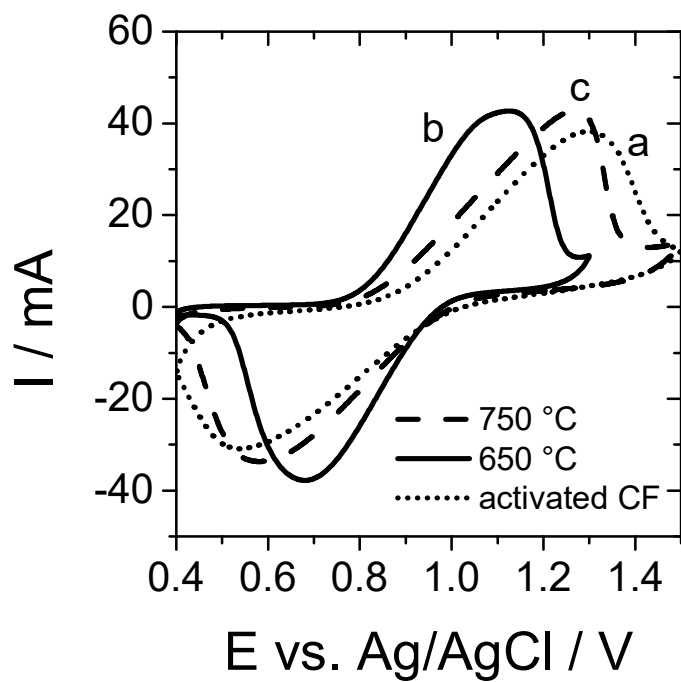


Figure 5

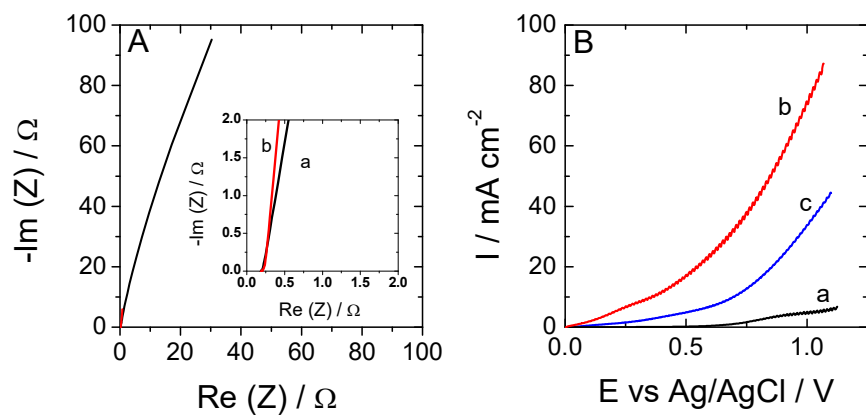


Figure 6

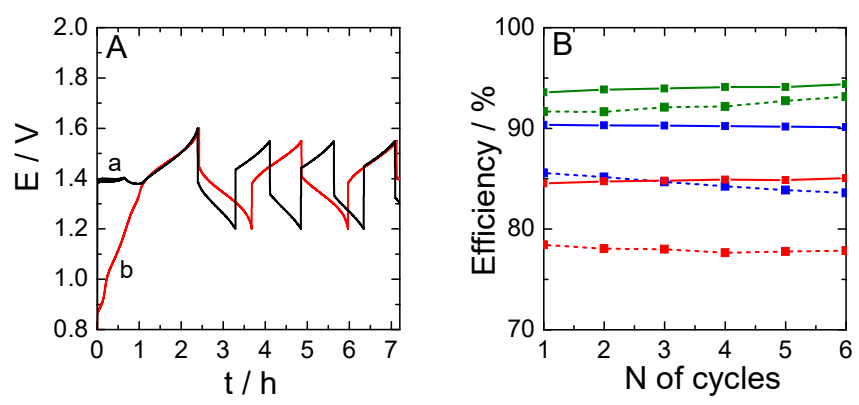


Figure 7

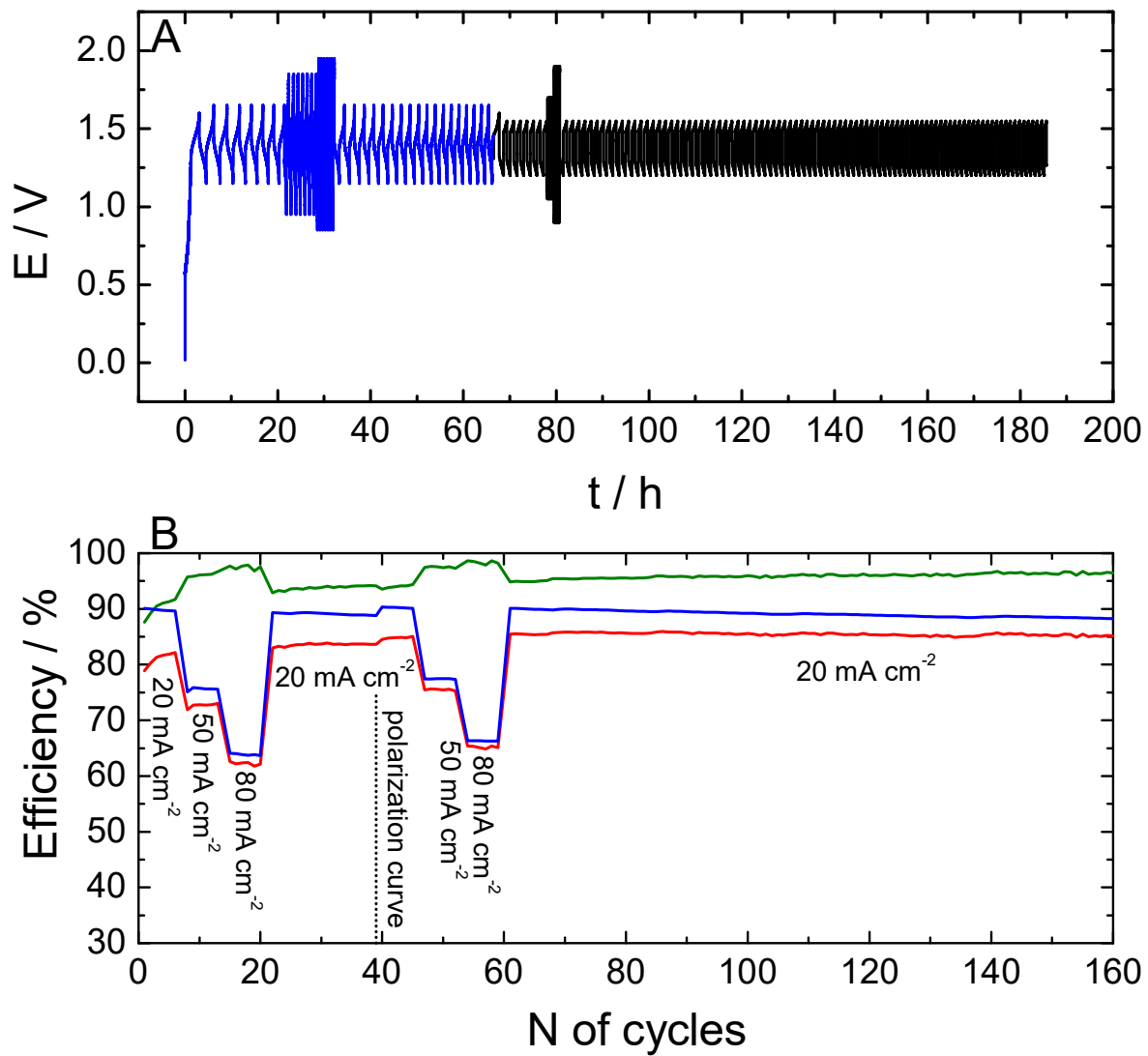


Figure 8

**Table 1** – Atomic concentration and carbon type (relative amounts expressed in %) of various graphite felt samples, as obtained from XPS analyses.

Sample	Atomic concentration (%)			Carbon type (%)		
	C	O	N	C sp <sup>2</sup>	C sp <sup>3</sup>	C-O
(a) Pristine GF	97.0	3.0	-	68.1	22.6	9.4
(b) Activated GF	94.3	5.7	-	62.5	27.2	10.3
(c) Activated GF modified with 10 PEI-PAA(MWCNT) bi-layers and pyrolysed at 650 °C under N <sub>2</sub>	92.0	6.0	2.0	73.3	19.3	7.4